

Intrinsic Kerr amplification for microwave electromechanics

Ermes Scarano, Elisabet K. Arvidsson, August K. Roos, Erik Holmgren, and David B. Haviland^{a)}

Department of Applied Physics, KTH Royal Institute of Technology, Hannes Alfvéns väg 12, SE-114 19 Stockholm, Sweden

(Dated: June 14, 2024)

Electromechanical transduction gain of 21 dB is realized in a micro-cantilever resonant force sensor operated in the unresolved-sideband regime. Strain-dependent kinetic inductance weakly couples cantilever motion to a superconducting nonlinear resonant circuit. A single pump generates motional sidebands and parametrically amplifies them via four-wave mixing. We study the gain and added noise, and we analyze potential benefits of this integrated amplification process in the context force sensitivity.

Keywords: kinetic inductance; parametric amplification; four-wave mixing; optomechanics; force sensing; strain

A resonant electromechanical transducer converts force to motion with a responsivity solely determined by its mechanical design. Cavity optomechanics offers an efficient scheme for measuring motion, but in many cases the transducer's overall sensitivity to force is limited by added noise in the measurement chain. In such cases the addition of a quantum-limited parametric amplifier can enhance sensitivity¹. Here we use the intrinsic Kerr nonlinearity of a superconducting microwave resonant circuit to achieve transduction gain in a micro-cantilever force sensor. However, for the device studied here, analysis of the noise revealed that this gain did not result in enhanced sensitivity to force.

In comparison to optical cavities, microwave circuits are appealing for their relative ease of integration with micro- and nano-electromechanical systems and their ability to achieve stronger electromechanical coupling. Since their first implementation^{1,2}, a large variety of superconducting microwave electromechanical devices have been studied and optimized for different goals³, such as a large single-photon coupling rate g_0 ⁴⁻⁷, electromechanical cooperativity \mathcal{C}^{8-10} , amplification^{11,12}, and efficient cooling of the mechanical mode¹³⁻¹⁹. Depending on the application, navigation of the design parameter space results in significantly different paths toward the goal.

Optimizing an electromechanical transducer for sensitivity to force constrains the mechanical resonator's shape, size, mass and resonance frequency. These constraints can conflict with other figures of merit. For example, a larger mass reduces the coupling rate g_0 and mechanical resonance frequency Ω_m , leading to operation in the unresolved-sideband regime and larger phonon occupation \bar{n}_m at a given temperature. Reduced g_0 can be compensated for with a stronger pump that increases the intracavity photon number \bar{n}_c , but superconducting circuits experience current-induced depairing that sets a limit on \bar{n}_c . This depairing results in a nonlinear inductance which is usually seen as a problem¹⁶. However, recent works exploit this nonlinearity for efficient cooling of the mechanical mode, both in the resolved¹⁸ and

unresolved²⁰ sideband regimes. The Kerr nonlinearity of kinetic inductance is also used for parametric amplification²¹ via three-wave or four-wave mixing processes^{22,23}.

In this paper we report on a microwave resonant circuit patterned from a thin film of niobium titanium nitride (Nb-Ti-N), which is weakly coupled to a micro-cantilever in the unresolved-sideband regime. We exploit the intrinsic Kerr nonlinearity of the superconducting circuit in a four-wave mixing process to realize 21 dB of transduction gain. We define the transduction gain as the ratio of the measured amplitude of the optomechanical motional sideband, normalized to that which would be produced by a linear cavity pumped to the same intracavity photon number.

In the cavity optomechanical transduction scheme, mechanical fluctuations with average phonon number \bar{n}_m are imprinted on the optical spectrum leaking out of the cavity, appearing as motional noise sidebands around the cavity pump frequency. In microwave electromechanics, the signal leaking from a resonant circuit into a transmission line is amplified before being demodulated and typically the added noise of this amplifier is the limiting factor degrading force sensitivity. Force sensitivity is expressed as a minimum detectable force F_{\min} , i.e. the force per unit bandwidth detected at unity signal-to-noise ratio. This definition accounts for actual force noise from the environment and the backaction of measurement, as well as added photon shot noise and amplification noise n_{add} expressed as an equivalent force noise²⁴. The normalized force sensitivity is given by

$$\frac{F_{\min}}{F_{\text{SQL}}} = \sqrt{\underbrace{\left(\bar{n}_m + \frac{1}{2}\right)}_{\text{Mechanics}} + \underbrace{|\mathcal{C}_{\text{eff}}|}_{\text{Backaction}} + \underbrace{\frac{1}{16|\mathcal{C}_{\text{eff}}|}}_{\text{Shot noise}} + \underbrace{\frac{n_{\text{add}}}{8|\mathcal{C}_{\text{eff}}|}}_{\text{Amplifier noise}}}, \quad (1)$$

where $F_{\text{SQL}} = \sqrt{2m_{\text{eff}}\Gamma\hbar\Omega_m}$ is the force sensitivity at the standard quantum limit (SQL), set by the resonators internal loss rate Γ and effective mass m_{eff} . Measurement induces noise, which translates to force through the effective cooperativity \mathcal{C}_{eff} ²⁴. In the unresolved-sideband regime the effective cooperativity can be approximated to,

$$\mathcal{C}_{\text{eff}}(\bar{n}_c) = \frac{1}{(1 - 2i\omega/\kappa)^2} \frac{4g_0^2\bar{n}_c}{\kappa\Gamma} \simeq \frac{4g_0^2\bar{n}_c}{\kappa\Gamma}, \quad (2)$$

^{a)}Electronic mail: haviland@kth.se

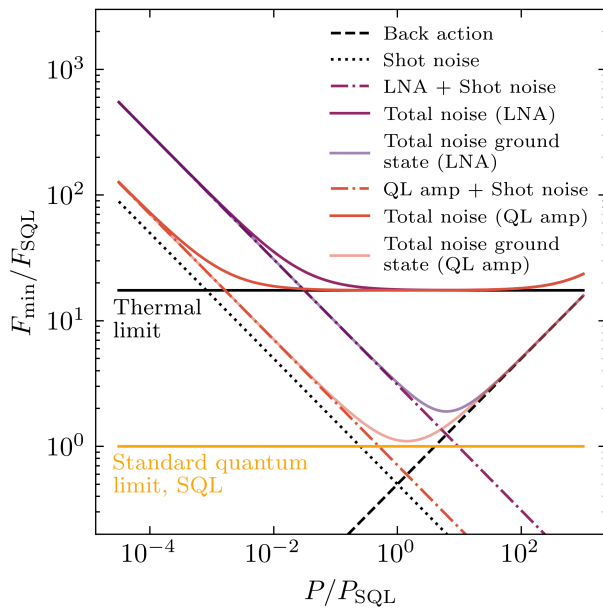


FIG. 1. Force sensitivity on mechanical resonance versus input power, both normalized to that at the standard quantum limit. The total force sensitivity (solid lines) is given by the mechanical fluctuations, backaction noise, as well as the force-equivalent shot noise and added amplifier noise. The effect of an additional stage of amplification is shown, either for a thermal state ($\bar{n}_m = 304$) or the quantum ground state of the mechanical mode.

where κ is total loss rate of the cavity. Figure 1 shows each contribution of Eqn. (1) as a function of input power P and their overall effect on sensitivity. Here P_{SQL} is the applied microwave power when the measurement is at the standard quantum limit, where shot noise and backaction noise are equal, corresponding to $C_{\text{eff}} = 1/4$. For input power below P_{SQL} , the added noise of the first stage of amplification limits force sensitivity. For example, in Fig. 1 we show the contribution from a cryogenic low-noise amplifier (LNA) with an equivalent noise temperature of 4 K. At 4.5 GHz this correspond to approximately $n_{\text{LNA}} = 19$ photons, deteriorating the force sensitivity so that detection at SQL is no longer possible and the optimal sensitivity is achieved for powers $P > P_{\text{SQL}}$.

Cantilevers operating in cryogenic environments typically have mechanical resonance frequencies that put the mechanical mode in a thermal state with $\bar{n}_m \approx k_{\text{B}}T/h\Omega_m \gg 1$. Figure 1 shows that, compared to the standard quantum limit, the thermally noise-limited case has an extended interval of power where force sensitivity is nearly constant and solely determined by the properties of the mechanical resonator. However, the nonlinearity of superconducting microwave circuits commonly limit \bar{n}_c , which, together with a small coupling rate g_0 , result in a situation where force sensitivity is instead limited by the added noise of a subsequent LNA. As shown in Fig. 1, one may improve the force sensitivity by adding a

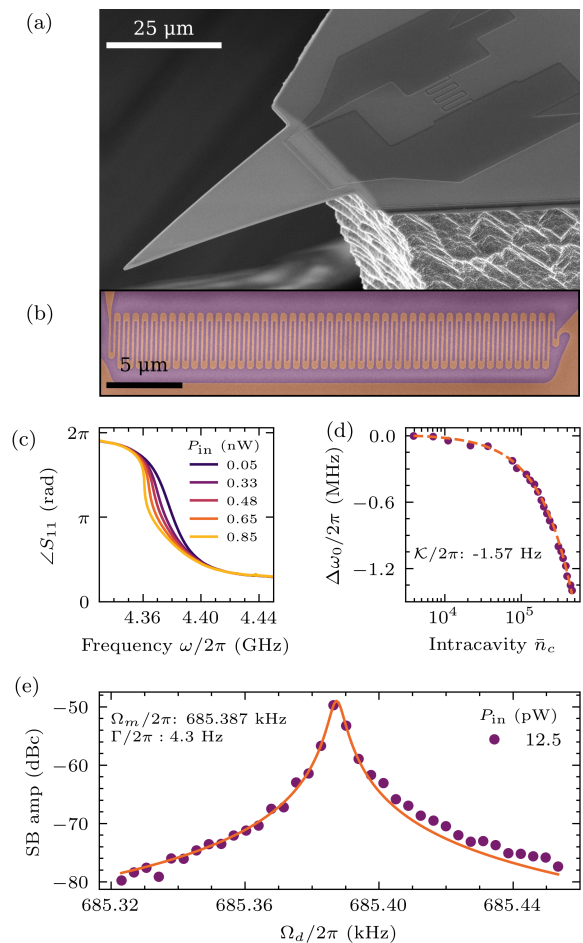


FIG. 2. Scanning electron microscope (SEM) image of (a) the cantilever and (b) the 100 nm-wide meandering nanowire inductor. The cantilever is formed from a 600 nm-thick silicon nitride plate and the nanowire is etched from a 15 nm-thin film of Nb-Ti-N. (c) Phase versus frequency of the microwave resonance for increasing input power P_{in} . The resonance frequency of the cavity ω_0 shifts to lower frequencies with increasing P_{in} , typical of a resonator with a Kerr-type nonlinearity. (d) The shift in resonance frequency $\Delta\omega_0$ as a function of intracavity photon number \bar{n}_c for a pump blue-detuned by approximately 50 MHz. For each pump power, ω_0 is measured by sweeping a weak probe tone through resonance. The Kerr coefficient is $\mathcal{K}/2\pi = -1.57$ Hz/photon. (e) Mechanical susceptibility measured from the driven motional sideband with resonant pumping in the linear regime of the cavity. The sideband amplitude is expressed in decibel with respect to the measured response at the carrier pump frequency (dBc).

quantum-limited amplifier between the resonant circuit, hereafter called “cavity”, and the LNA. For a sufficiently high-gain phase-preserving quantum-limited parametric amplifier, the number of added photons by the amplifier to the measurement is given by $n_{\text{PA}} = 1/2$ ²⁵. Yet adding a separate quantum-limited amplifier comes at significant

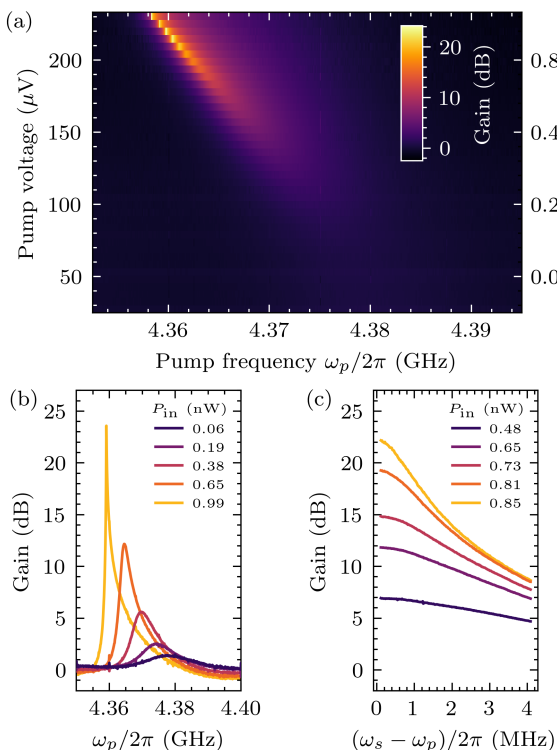


FIG. 3. (a) Four-wave mixing parametric gain of an injected signal tone ω_s as a function of pump frequency ω_p and pump power P_{in} at fixed detuning $(\omega_s - \omega_p)/2\pi = 685.386$ kHz. (b) Signal gain versus ω_p at various pump power. (c) Gain versus ω_s for various ω_p and P_{in} along the ridge of maximum gain in (a).

cost in complexity and more complicated operation, including an additional pump, pump-cancellation tone, as well as additional isolators and associated cabling¹⁴. In our work, we investigate a simpler implementation where a nonlinear cavity is not only used for transduction of motion to measured signal, but also for amplification, i.e. with one pump both generating and amplifying the motional sidebands.

We demonstrate this implementation with the device shown in Fig. 2(a). The cantilever force sensor is tightly integrated with a compact microwave circuit consisting an interdigitated capacitor in series with a long meandering nanowire having large kinetic inductance. The nanowire has width 100 nm and thickness 15 nm, and it meanders along the base of the cantilever, as shown in detail in the false-color micrograph Fig. 2(b). The silicon nitride (Si-N) micro-cantilever has a fundamental bending mode with resonance frequency $\Omega_m/2\pi = 685.387$ kHz and linewidth $\Gamma/2\pi = 4.3$ Hz. The microwave cavity with resonance frequency $\omega_0/2\pi = 4.378$ GHz is strongly overcoupled to the transmission line, having total linewidth $\kappa/2\pi = 21.18$ MHz, corresponding to a loaded quality factor of $Q = 206.7$. Can-

tilever bending generates surface strain which is maximum at the line where the cantilever meets the silicon substrate. This strain changes the nanowire's kinetic inductance, shifting the cavity resonance and thereby realizing electromechanical mode coupling^{26,27}. For purely geometric coupling where the kinetic inductance per unit length is assumed constant, simulations of the strain²⁸ result in a single-photon coupling strength $g_0 \approx 50$ mHz, giving an effective cooperativity of $\mathcal{C}_{eff} \approx 10^{-4}$ at intracavity photon number $\bar{n}_c = 10^6$.

Figure 2(c) shows the phase response of the cavity as a function of frequency and power measured in a dilution refrigerator at $T = 10$ mK. The phase of the reflected signal changes by 2π when sweeping through resonance, characteristic of an overcoupled resonator measured in reflection. Increasing power shifts the resonance frequency to lower values and the phase response sharpens, as expected from a current-induced pair-breaking nonlinear inductance. Such behavior is approximated to leading order by a Kerr-type nonlinearity, where the Kerr coefficient \mathcal{K} describes the strength of the nonlinearity in terms of a frequency shift per photon. We measure the shift of the cavity resonance frequency as a function of intracavity photon number \bar{n}_c , by varying the power of a blue-detuned pump while sweeping a much weaker probe tone through resonance. Figure 2(d) shows the result of this measurement and the linear fit to determine a Kerr coefficient $\mathcal{K}/2\pi = -1.57$ Hz/photon for our device.

We operate the nonlinear cavity as a four-wave mixing parametric amplifier²⁹ and analyze the gain \mathcal{G} by injecting a single probe tone at ω_s , blue-detuned by Ω_m from a strong pump tone at ω_p . The amplifier bandwidth is smaller than the cavity linewidth κ and it decreases with increasing gain (pump power). We therefore intentionally designed the cavity with a relatively large κ (low Q) to operate in the unresolved-sideband regime, ensuring high gain at detuning Ω_m . Figures 3(a) and (b) show the measured gain versus pump frequency for various pump powers, obtained by sweeping both pump and probe frequency with fixed separation $\omega_s - \omega_p = \Omega_m$. For increasing pump power the gain peak shifts to lower frequency, as expected for a negative Kerr coefficient. For our device, we reach $\mathcal{G} \approx 24$ dB for the largest pump power before the cavity bifurcates and the gain degrades. Figure 3(c) shows the gain and bandwidth for selected pump powers, measured by fixing ω_p at the previously determined maximum gain for each power, and sweeping the signal tone ω_s .

To demonstrate transduction gain, we repeat the sweep over pump power and pump frequency, now driving the cantilever through a piezoelectric shaker. The cantilever motion generates sidebands in the upconverted spectrum, at either side of ω_p . Since two sidebands are generated, the gain will be sensitive to their relative phase, which is determined by the properties of the cavity. However, in the unresolved-sideband regime, this relative phase is such that transduction gain is observed³⁰. To capture the motion spectrum we use a multifrequency lockin to excite

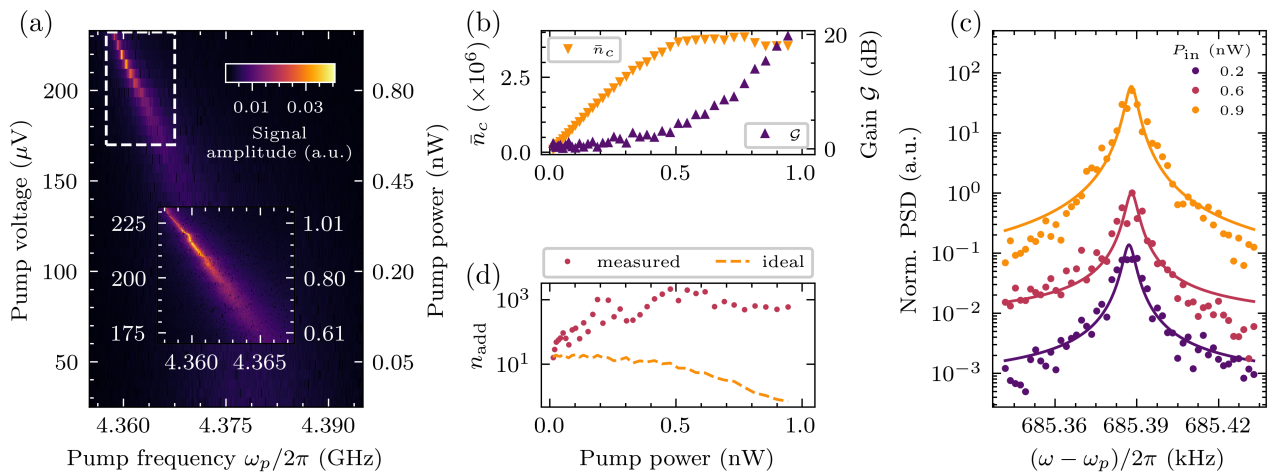


FIG. 4. (a) Parametric amplification of an upconverted motional sideband when the mechanical mode is driven with a frequency comb. The area under the motional sideband is plotted as a function of pump frequency ω_p and pump amplitude/power, normalized to the input amplitude. Increasing the pump power shifts the cavity's resonance frequency and amplifies the response at the motional sideband. (Inset) Zoom of the dashed box with finer stepping, highlighting the ridge of maximum response. (b) Transduction gain \mathcal{G} and \bar{n}_c at multiple pump powers along the ridge of maximum sideband response in (a). (c) Fluctuations of the undriven mechanical mode measured at the upper motional sideband for three pump powers with ω_p placed on the ridge of maximum gain. The power spectral density (PSD) is normalized to the intracavity photon number \bar{n}_c . (d) Measured n_{add} and that expected for a quantum limited parametric amplifier followed by the LNA.

the cantilever with a tuned frequency comb with equal amplitudes, and phases chosen to reduce peak excitation in the time domain (see Supplementary Material). The lockin measures the response at the upconverted comb frequencies, capturing the mechanical motion spectrum in a single measurement time window. Fitting a model composed of a Lorentzian with a frequency-independent added noise to the data, we extract the area under the sideband, proportional to the amplitude spectrum of the drive mechanical displacement. Fig. 4(a) shows the integrated sideband response normalized to the input amplitude, from which we identify the frequency of maximum response for each pump power.

Maximum transduction gain follows a ridge in pump power and frequency, as expected for parametric gain generated close to bifurcation. Figure 4(b) shows the transduction gain \mathcal{G} and \bar{n}_c versus pump power, where pump frequency is adjusted to follow the ridge of maximum sideband response. We determine \bar{n}_c using methods described in Ref.¹⁸. At each pump power, the amplified signal is the integrated sideband power spectrum, normalized to \bar{n}_c . The transduction gain is given by the ratio of this amplified signal, to that in the low power regime, where $\mathcal{G} \equiv 1$. For a detailed description see the supplementary material.

Operating the sensor on this ridge of maximum gain, we are able to resolve the amplified motional noise of the undriven cantilever, as shown in Fig. 4(c). The plotted data are an average of ten consecutive Power Spectral Densities (PSDs) measured with resolution bandwidth 1.86 Hz. The solid lines represent the best fit of a model

comprised of a Lorentzian plus white added noise. Averaging over 100 consecutive fits, we extract the added noise expressed as equivalent photon number, as shown in Fig. 4(d).

The ideal phase-insensitive parametric amplifier would result in a reduction of the added noise with increasing gain, approaching $n_{add} = 1/2$ at high gain [dashed curve in Fig. 4(d)] as described by

$$n_{add} = n_{PA} + \frac{n_{LNA}}{\mathcal{G}}. \quad (3)$$

However, we observe instead an increase in the added noise. Possible explanations of this additional noise could be nonlinear loss mechanisms in the cavity, for example increased quasiparticle losses associated with the current-induced pair-breaking nonlinearity, or heating of the cavity by the pump³¹.

The use of a nonlinear cavity to parametrically amplify the motional sidebands also results in increased backaction noise, due to the amplification of the intracavity fluctuations³². In contrast, a cold isolator screens the cavity from this backaction when using a separate parametric amplifier¹. The potential improvements in the resulting force sensitivity are contingent upon the effective cooperativity. In the case considered here $\mathcal{C}_{eff} \ll 1/4$ such amplified backaction is negligible at the observed level of gain.

In conclusion, we described a micro-cantilever force-sensor with a compact and integrated microwave cavity. The sensor employed kinetic inductive electromechanical coupling to realize force transduction, and the nonlin-

earity of the superconducting cavity was used for parametric amplification. The measurement configuration required only a single pump to combine these two effects, achieving up to 21 dB transduction gain of the electromechanical motional sidebands. However, noise analysis revealed that this gain did not come with an improvement in signal-to-noise ratio, most likely due to nonlinear loss mechanisms or heating by the pump. It is possible to mitigate these effects by designing for higher Kerr coefficient through a thinner superconducting film (lower critical current) or through a shorter nanowire (larger current for given \bar{n}_c). Further study of this sensor concept is required to determine under which circumstances this gain mechanism can be exploited for improved force sensitivity.

SUPPLEMENTARY MATERIAL

See the Supplementary Material for details on the multifrequency lockin measurement technique with a tuned frequency comb driving the mechanical oscillator, determination of the \mathcal{K} coefficient with two tone spectroscopy and analysis of the intracavity photon number and transduction gain.

ACKNOWLEDGEMENTS

We acknowledge funding from the European Union Horizon 2020 EIC Pathfinder Grant Agreement No. 828966 — QAFM and the Swedish SSF Grant No. ITM17-0343 supported this work. We thank the Quantum-Limited Atomic Force Microscopy (QAFM) team for fruitful discussions: T. Glatzel, M. Zutter, E. Tholén, D. Forchheimer, I. Ignat, M. Kwon, and D. Platz. We particularly thank anonymous reviewer 2 whose careful reading and thoughtful comments helped to substantially improve the paper.

AUTHOR DECLARATIONS

Conflict of Interest

The authors have no conflicts to disclose.

Author Contributions

Ermes Scarano: Conceptualization (equal); Investigation (lead); Formal Analysis (equal); Visualization (equal); Writing – original draft (lead); Writing – review and editing (equal). **Elisabet K. Arvidsson:** Conceptualization (equal); Investigation (supporting); Formal Analysis (equal); Visualization (equal); Writing – original draft (supporting); Writing – review and editing (equal). **August K. Roos:** Conceptualization (equal);

Investigation (supporting); Formal Analysis (supporting); Visualization (equal); Writing – original draft (supporting); Writing – review and editing (supporting). **Erik Holmgren:** Supervision (supporting). **David B. Haviland:** Conceptualization (equal); Funding acquisition (lead); Resources (lead); Project administration (lead); Supervision (lead); Writing – original draft (supporting); Writing – review and editing (equal).

DATA AVAILABILITY

The data that support the findings of this study are openly available in Zenodo at <https://doi.org/10.5281/zenodo.11656972>, reference number 11656972.

- ¹J. D. Teufel, T. Donner, M. A. Castellanos-Beltran, J. W. Harlow, and K. W. Lehnert. Nanomechanical motion measured with an imprecision below that at the standard quantum limit. *Nature Nanotechnology*, 4(12):820–823, Dec 2009. ISSN 1748-3395. doi:10.1038/nnano.2009.343. URL <https://doi.org/10.1038/nnano.2009.343>.
- ²C. A. Regal, J. D. Teufel, and K. W. Lehnert. Measuring nanomechanical motion with a microwave cavity interferometer. *Nature Physics*, 4(7):555–560, Jul 2008. ISSN 1745-2481. doi:10.1038/nphys974. URL <https://doi.org/10.1038/nphys974>.
- ³Markus Aspelmeyer, Tobias J. Kippenberg, and Florian Marquardt. Cavity optomechanics. *Rev. Mod. Phys.*, 86:1391–1452, Dec 2014. doi:10.1103/RevModPhys.86.1391. URL <https://link.aps.org/doi/10.1103/RevModPhys.86.1391>.
- ⁴P. D. Nation, J. Suh, and M. P. Blencowe. Ultrastrong optomechanics incorporating the dynamical casimir effect. *Phys. Rev. A*, 93:022510, Feb 2016. doi:10.1103/PhysRevA.93.022510. URL <https://link.aps.org/doi/10.1103/PhysRevA.93.022510>.
- ⁵A. P. Reed, K. H. Mayer, J. D. Teufel, L. D. Burkhardt, W. Pfaff, M. Reagor, L. Sletten, X. Ma, R. J. Schoelkopf, E. Knill, and K. W. Lehnert. Faithful conversion of propagating quantum information to mechanical motion. *Nature Physics*, 13(12):1163–1167, Dec 2017. ISSN 1745-2481. doi:10.1038/nphys4251. URL <https://doi.org/10.1038/nphys4251>.
- ⁶I. C. Rodrigues, D. Bothner, and G. A. Steele. Coupling microwave photons to a mechanical resonator using quantum interference. *Nature Communications*, 10(1):5359, Nov 2019. ISSN 2041-1723. doi:10.1038/s41467-019-12964-2. URL <https://doi.org/10.1038/s41467-019-12964-2>.
- ⁷D. Zoepfl, M. L. Juan, C. M. F. Schneider, and G. Kirchmair. Single-photon cooling in microwave magnetomechanics. *Phys. Rev. Lett.*, 125:023601, Jul 2020. doi:10.1103/PhysRevLett.125.023601. URL <https://link.aps.org/doi/10.1103/PhysRevLett.125.023601>.
- ⁸G. A. Peterson, S. Kotler, F. Lecocq, K. Cicak, X. Y. Jin, R. W. Simmonds, J. Aumentado, and J. D. Teufel. Ultrastrong parametric coupling between a superconducting cavity and a mechanical resonator. *Phys. Rev. Lett.*, 123:247701, Dec 2019. doi:10.1103/PhysRevLett.123.247701. URL <https://link.aps.org/doi/10.1103/PhysRevLett.123.247701>.
- ⁹Hengjiang Ren, Matthew H. Matheny, Gregory S. MacCabe, Jie Luo, Hannes Pfeifer, Mohammad Mirhosseini, and Oskar Painter. Two-dimensional optomechanical crystal cavity with high quantum cooperativity. *Nature Communications*, 11(1):3373, Jul 2020. ISSN 2041-1723. doi:10.1038/s41467-020-17182-9. URL <https://doi.org/10.1038/s41467-020-17182-9>.
- ¹⁰Alkim Bozkurt, Han Zhao, Chaitali Joshi, Henry G. LeDuc, Peter K. Day, and Mohammad Mirhosseini. A quantum electromechanical interface for long-lived phonons. *Nature Physics*, 19(9):1326–1332, Sep 2023. ISSN 1745-2481. doi:10.1038/s41567-023-02080-w. URL <https://doi.org/10.1038/s41567-023-02080-w>.

- ¹¹D. Cattiaux, X. Zhou, S. Kumar, I. Golokolenov, R. R. Gazizulin, A. Luck, L. Mercier de Lépinay, M. Sillanpää, A. D. Armour, A. Fefferman, and E. Collin. Beyond linear coupling in microwave optomechanics. *Phys. Rev. Res.*, 2:033480, Sep 2020. doi:10.1103/PhysRevResearch.2.033480. URL <https://link.aps.org/doi/10.1103/PhysRevResearch.2.033480>.
- ¹²Junghyun Shin, Younghun Ryu, Mohammad-Ali Miri, Seung-Bo Shim, Hyungsoon Choi, Andrea Alù, Junho Suh, and Jinwoong Cha. On-chip microwave frequency combs in a superconducting nanoelectromechanical device. *Nano Letters*, 22(13):5459–5465, 2022. doi:10.1021/acs.nanolett.2c01503. URL <https://doi.org/10.1021/acs.nanolett.2c01503>. PMID: 35708318.
- ¹³M. P. Blencowe and E. Buks. Quantum analysis of a linear dc squid mechanical displacement detector. *Phys. Rev. B*, 76:014511, Jul 2007. doi:10.1103/PhysRevB.76.014511. URL <https://link.aps.org/doi/10.1103/PhysRevB.76.014511>.
- ¹⁴J. D. Teufel, T. Donner, Dale Li, J. W. Harlow, M. S. Allman, K. Cicak, A. J. Sirois, J. D. Whittaker, K. W. Lehnert, and R. W. Simmonds. Sideband cooling of micromechanical motion to the quantum ground state. *Nature*, 475(7356):359–363, Jul 2011. ISSN 1476-4687. doi:10.1038/nature10261. URL <https://doi.org/10.1038/nature10261>.
- ¹⁵Amir H. Safavi-Naeini, Jasper Chan, Jeff T. Hill, Thiago P. Mayer Alegre, Alex Krause, and Oskar Painter. Observation of quantum motion of a nanomechanical resonator. *Phys. Rev. Lett.*, 108:033602, Jan 2012. doi:10.1103/PhysRevLett.108.033602. URL <https://link.aps.org/doi/10.1103/PhysRevLett.108.033602>.
- ¹⁶Mingyun Yuan, Vibhor Singh, Yaroslav M. Blanter, and Gary A. Steele. Large cooperativity and microkelvin cooling with a three-dimensional optomechanical cavity. *Nature Communications*, 6(1):8491, 10 2015. ISSN 2041-1723. doi:10.1038/ncomms9491. URL <https://doi.org/10.1038/ncomms9491>.
- ¹⁷D. Cattiaux, I. Golokolenov, S. Kumar, M. Sillanpää, L. Mercier de Lépinay, R. R. Gazizulin, X. Zhou, A. D. Armour, O. Bourgeois, A. Fefferman, and E. Collin. A macroscopic object passively cooled into its quantum ground state of motion beyond single-mode cooling. *Nature Communications*, 12(1):6182, Oct 2021. ISSN 2041-1723. doi:10.1038/s41467-021-26457-8. URL <https://doi.org/10.1038/s41467-021-26457-8>.
- ¹⁸Daniel Bothner, Ines C. Rodrigues, and Gary A. Steele. Four-wave-cooling to the single phonon level in Kerr optomechanics. *Communications Physics*, 5(1):33, Feb 2022. ISSN 2399-3650. doi:10.1038/s42005-022-00808-3. URL <https://doi.org/10.1038/s42005-022-00808-3>.
- ¹⁹Yannick Seis, Thibault Capelle, Eric Langman, Sampo Saarinen, Eric Planz, and Albert Schliesser. Ground state cooling of an ultracoherent electromechanical system. *Nature Communications*, 13(1):1507, Mar 2022. ISSN 2041-1723. doi:10.1038/s41467-022-29115-9. URL <https://doi.org/10.1038/s41467-022-29115-9>.
- ²⁰D. Zoepfl, M. L. Juan, N. Diaz-Naufal, C. M. F. Schneider, L. F. Deeg, A. Sharafiev, A. Metelmann, and G. Kirchmair. Kerr enhanced backaction cooling in magnetomechanics. *Phys. Rev. Lett.*, 130:033601, Jan 2023. doi:10.1103/PhysRevLett.130.033601. URL <https://link.aps.org/doi/10.1103/PhysRevLett.130.033601>.
- ²¹Jonas Zmuidzinias. Superconducting microresonators: Physics and applications. *Annual Review of Condensed Matter Physics*, 3(1):169–214, 2012. doi:10.1146/annurev-conmatphys-020911-125022. URL <https://doi.org/10.1146/annurev-conmatphys-020911-125022>.
- ²²M. R. Vissers, R. P. Erickson, H.-S. Ku, Leila Vale, Xian Wu, G. C. Hilton, and D. P. Pappas. Low-noise kinetic inductance traveling-wave amplifier using three-wave mixing. *Applied Physics Letters*, 108(1):012601, 01 2016. ISSN 0003-6951. doi:10.1063/1.4937922. URL <https://doi.org/10.1063/1.4937922>.
- ²³R. P. Erickson and D. P. Pappas. Theory of multiwave mixing within the superconducting kinetic-inductance traveling-wave amplifier. *Phys. Rev. B*, 95:104506, Mar 2017. doi:10.1103/PhysRevB.95.104506. URL <https://link.aps.org/doi/10.1103/PhysRevB.95.104506>.
- ²⁴W.P. Bowen and G.J. Milburn. *Quantum Optomechanics*. Taylor & Francis, Boca Raton, first edition, 2015. ISBN 9781482259155. URL <https://doi.org/10.1201/b19379>.
- ²⁵Carlton M. Caves. Quantum limits on noise in linear amplifiers. *Phys. Rev. D*, 26:1817–1839, Oct 1982. doi:10.1103/PhysRevD.26.1817. URL <https://link.aps.org/doi/10.1103/PhysRevD.26.1817>.
- ²⁶August K. Roos, Ermes Scarano, Elisabet K. Arvidsson, Erik Holmgren, and David B. Haviland. Kinetic inductive electromechanical transduction for nanoscale force sensing. *Phys. Rev. Appl.*, 20:024022, 08 2023. doi:10.1103/PhysRevApplied.20.024022. URL <https://link.aps.org/doi/10.1103/PhysRevApplied.20.024022>.
- ²⁷Ermes Scarano, Elisabet K. Arvidsson, August K. Roos, Erik Holmgren, and David B. Haviland. Temperature dependence of microwave losses in lumped-element resonators made from superconducting nanowires with high kinetic inductance, 2024.
- ²⁸August K. Roos. *Superconducting kinetic inductance devices for nanoscale force sensing*. PhD thesis, KTH, Nanostructure Physics, 2024. QC 2024-02-06.
- ²⁹Alexander Anferov, Aziza Suleymanzade, Andrew Oriani, Jonathan Simon, and David I. Schuster. Millimeter-wave four-wave mixing via kinetic inductance for quantum devices. *Phys. Rev. Appl.*, 13:024056, Feb 2020. doi:10.1103/PhysRevApplied.13.024056. URL <https://link.aps.org/doi/10.1103/PhysRevApplied.13.024056>.
- ³⁰M. Hatridge, R. Vijay, D. H. Slichter, John Clarke, and I. Siddiqi. Dispersive magnetometry with a quantum limited squid parametric amplifier. *Phys. Rev. B*, 83:134501, Apr 2011. doi:10.1103/PhysRevB.83.134501. URL <https://link.aps.org/doi/10.1103/PhysRevB.83.134501>.
- ³¹M. Malnou, M.R. Vissers, J.D. Wheeler, J. Aumentado, J. Hubmayr, J.N. Ullom, and J. Gao. Three-wave mixing kinetic inductance traveling-wave amplifier with near-quantum-limited noise performance. *PRX Quantum*, 2:010302, Jan 2021. doi:10.1103/PRXQuantum.2.010302. URL <https://link.aps.org/doi/10.1103/PRXQuantum.2.010302>.
- ³²Ines Corveira Rodrigues, Gary Alexander Steele, and Daniel Bothner. Parametrically enhanced interactions and nonreciprocal bath dynamics in a photon-pressure Kerr amplifier. *Science Advances*, 8(34):eabq1690, 2022. doi:10.1126/sciadv.abq1690. URL <https://www.science.org/doi/abs/10.1126/sciadv.abq1690>.

Supplementary Material:

Intrinsic Kerr amplification for microwave electromechanics

Ermes Scarano, Elisabet K. Arvidsson, August K. Roos, Erik Holmgren, and David B. Haviland^{a)}

Department of Applied Physics, KTH Royal Institute of Technology, Hannes Alfvéns väg 12, SE-114 19 Stockholm, Sweden

(Dated: June 14, 2024)

SUPPLEMENTARY MATERIAL 1: MULTIFREQUENCY LOCKIN MEASUREMENT

The linear response function of a system, e.g. the mechanical susceptibility of an eigenmode of a cantilever, can be determined by stepping a single drive tone through resonance while measuring the amplitude and phase of the response at the drive frequency using the lockin technique. To properly resolve the Lorentzian lineshape the step size Δf should be smaller or on the order of the linewidth γ_m , and the signal must be integrated with a bandwidth $\delta f \leq \Delta f$. Tuning the discrete set of stepped frequencies $f_i = n_i \Delta f$, to be integer multiples of the integration bandwidth $\Delta f = m \delta f$, where n_i, m are positive integers, ensures that no Fourier leakage will occur. The measurement time for a set of N frequencies will be $T = N/\delta f$.

A much faster measurement is achieved by driving the system with a frequency comb, i.e. simultaneously applying all the drive tones at the multiple frequencies f_i . The multifrequency method reduces the measurement time to $T = 1/\delta f$. By tuning the frequencies in the comb to be integer multiples of δf , the drive signal in the time domain is periodic with $T = 1/\delta f$ and a common reference for the phases of all tones can be defined, as in a Discrete Fourier Transform. The response to this multifrequency drive will be identical to stepping a single-frequency drive, as long as the system remains linear under the applied drive signal.

A frequency comb with large number of tones can drive the system in to a nonlinear regime at that point in time when the waveform peaks, when the amplitudes at all frequencies align with the same phase. The peak value can be reduced with proper choice of the phases. The worst case is that of equal phases for all the tones, where the drive signal in the time domain is a sinc pulse. For arbitrary number of frequencies, there is no analytical solution to obtain the minimum *crest factor*, defined as the ratio of the peak to the root-mean-square value of the waveform³. To avoid nonlinear response of the cantilever in our measurement, we drove the mechanical resonator with a comb of nine frequencies and we chose the drive phases by generating multiple sets of random phases, selecting the waveform with the lowest crest factor.

SUPPLEMENTARY MATERIAL 2: DETERMINING THE KERR COEFFICIENT

In Fig. 2(d) of the main text we determine the Kerr coefficient by considering the shift of the cavity's resonance frequency ω_0 as a function of intracavity photon number \bar{n}_c . Intracavity photons are produced by a pump tone at the frequency ω_p which is blue-detuned from ω_0 by $\Delta = 50$ MHz, larger than the cavity linewidth $\Delta > \kappa$. The corresponding number of intracavity photons circulating in the resonator is given by:

$$\bar{n}_c = \frac{P_{in}}{\hbar\omega_p} \frac{\kappa_{ext}}{\kappa^2/4 + \Delta^2} \quad (S1)$$

The response phase in Fig. S1(a) is measured by two-tone spectroscopy, with a pump tone at a fixed frequency and a weak probe tone stepping through the cavity resonance. The zoom details the shift of resonance frequency with increasing pump power. The shifted resonance frequency is a linear function of intracavity photon number, with slope corresponding to twice the Kerr coefficient \mathcal{K} , as shown in Fig. S1(b).

^{a)}Electronic mail: haviland@kth.se

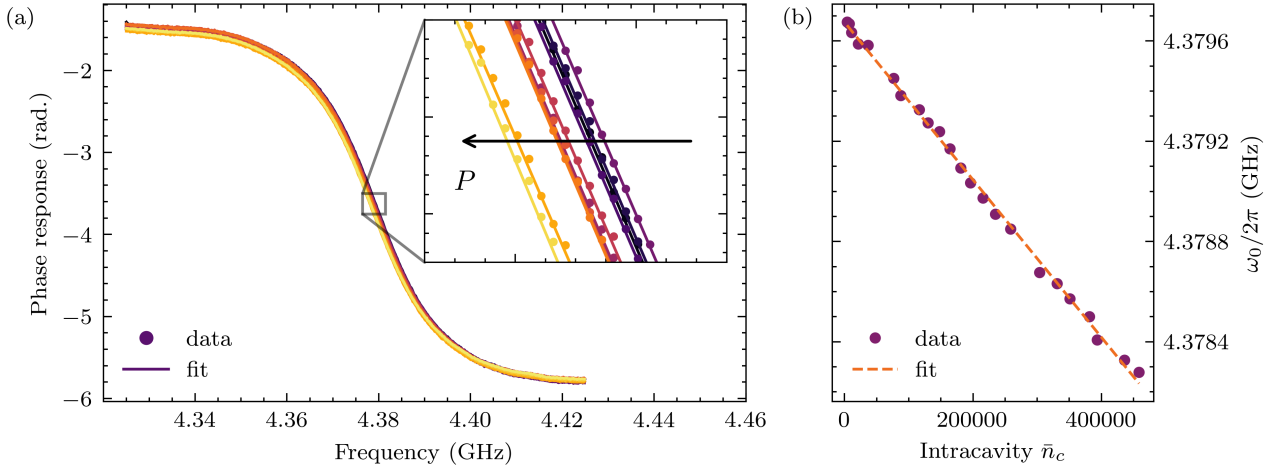


FIG. S1. (a) Measured response phase versus frequency of the weak probe tone, plotted for various power of a strong blue-detuned pump tone. The pump is fixed at a frequency detuned by 50 MHz from ω_0 . The input pump power P_{in} ranges from -81 dBm to -60 dBm. The inset shows a zoom detailing the small decrease in resonance frequency ω_0 for increasing pump power (direction indicated by arrow). (b) The shifted resonance frequency as a function of intracavity photons \bar{n}_c , from which we extract $\mathcal{K} = (-1.572 \pm 0.017)$ Hz/photon

SUPPLEMENTARY MATERIAL 3: CALCULATING INTRACAVITY PHOTONS

We follow the methods outlined in the Supplementary Methods of Ref.⁴ to determine the number of circulating photons \bar{n}_c in the cavity with a Kerr-type nonlinearity. The Kerr effect captures the strength of a nonlinearity in terms the Kerr coefficient \mathcal{K} which we can interpret as the frequency shift per intracavity photon. The equation of motion for the intracavity field a for a single port cavity measured in reflection, is given by

$$\dot{a} = \left[i(\omega_0 + \mathcal{K}|a|^2) - \frac{\kappa}{2} \right] a + \sqrt{\kappa_{\text{ext}}} a_{\text{in}}, \quad (\text{S2})$$

where ω_0 is the bare resonance frequency of the cavity, κ its total linewidth, κ_{ext} its external linewidth, and a_{in} photon field at the input of the cavity.

For a single-tone probe at frequency ω_p , the input field is given by $a_{\text{in}} = |\alpha_{\text{in}}| \exp(i\omega_p t)$. In this case, the intracavity field may be written as $a = \alpha \exp(i\omega_p t)$. Defining a detuning between drive tone and the bare resonance $\Delta = \omega_p - \omega_0$, the equation of motion may be written,

$$\alpha \left[\frac{\kappa}{2} + i(\Delta - \mathcal{K}\alpha^2) \right] = \sqrt{\kappa_{\text{ext}}} |\alpha_{\text{in}}|. \quad (\text{S3})$$

Multiplying Eqn. (S3) by its complex conjugate forms a third-order polynomial in $\bar{n}_c = \alpha^* \alpha$

$$\mathcal{K}^2 \bar{n}_c^3 - 2\mathcal{K}\Delta \bar{n}_c^2 + \left(\Delta^2 + \frac{\kappa^2}{4} \right) \bar{n}_c - \kappa_{\text{ext}} |\alpha_{\text{in}}|^2 = 0, \quad (\text{S4})$$

where the number of incoming photons is given by

$$n_{\text{in}} \equiv |\alpha_{\text{in}}|^2 = \frac{P_{\text{in}}}{\hbar\omega_p} \quad (\text{S5})$$

For each given value of pump power P_{in} and drive frequency ω_p , and the values of \mathcal{K} , and ω_0 , κ , κ_{ext} previously determined (in the linear regime), we numerically solve the polynomial Eqn. (S4) to arrive at \bar{n}_c . The polynomial has in general three roots, but our input power corresponds to a regime below bifurcation, where only one real root exists. With the derived value of the Kerr parameter we can reproduce the $S_{11}(\omega)$ curve for a swept pump tone (Fig. S2(a)). For the input-output relation $\langle a_{\text{out}} \rangle = \langle a_{\text{in}} \rangle - \sqrt{\kappa_{\text{ext}}} \langle a \rangle$, the reflection coefficient of the single port cavity is given by

$$S_{11} = \frac{\langle a_{\text{out}} \rangle}{\langle a_{\text{in}} \rangle} = 1 - \frac{\kappa_{\text{ext}}}{\kappa/2 + i(\Delta - \mathcal{K}a^2)} \quad (\text{S6})$$

with $\omega_0/2\pi = 4.3796$ GHz, $\kappa/2\pi \simeq \kappa_{\text{ext}}/2\pi = 24.186$ MHz, $\mathcal{K}/2\pi = -1.57$ Hz/photon.

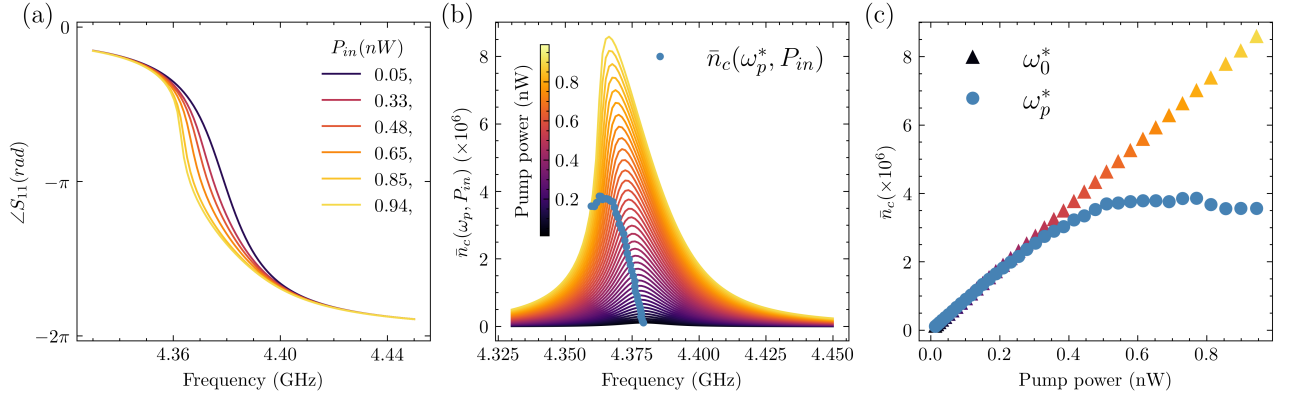


FIG. S2. (a) Reflection coefficient S_{11} vs frequency simulated from the Kerr model for the single tone solution in Eqn. (S6). This simulation matches well the measurements reported in Fig. 2(c) of the main text. (b) The number of intracavity photons \bar{n}_c as a function of pump frequency for various input pump power P_{in} . The smooth curves are calculated from the Kerr model. For each pump power a blue point marks the frequency ω_p^* corresponding to the measured maximum sideband signal. (c) Comparison between maximum \bar{n}_c and n_c for a pump frequency that corresponds to maximum gain.

SUPPLEMENTARY MATERIAL 4: DETERMINING THE TRANSDUCTION GAIN

The transduction gain as defined in the main text corresponds to the net amplification of the motional sideband, or increase in the amplitude of the response at the sideband frequency, in comparison with that which would be observed with a linear cavity. To determine the transduction gain from the experimental data (Fig. 4(a) in the main text), we first find the pump frequency ω_p^* at which we observe maximum sideband response, for each input pump power. This experimentally determined $\omega_p^*(P_{in})$ can be estimated analytically from the Kerr model as the frequency $\omega_0^*(P)$ at which the number of intracavity photons is maximum (see Fig. S2). The experimental $\omega_p^*(P_{in})$ does not coincide exactly with the analytical $\omega_0^*(P_{in})$ but is slightly red detuned, as shown in Fig. S2(b,c)

To calculate the value of the transduction gain G we assume that the power spectral density $S_{xx}(\Omega)$ of the mechanical displacement (either driven coherently, or with broad band noise) is independent on the microwave pump power and frequency. At the frequency of maximum sideband response corresponding to the j th input pump power $\omega_p^*(P_{in,j})$, the voltage power spectral density of the measured motional sidebands scales as:

$$S_{VV,j} \propto g_0 S_{xx} G_j \bar{n}_c(\omega_p^*, P_{in,j}). \quad (\text{S7})$$

In the low power regime ($P_{in,j} < 0.2$ nW) both S_{VV} and \bar{n}_c scale linearly with the input power, defining the regime where gain is unity. Therefore, at the j th power the gain is:

$$G_j = \frac{S_{VV,j}/\bar{n}_c(\omega_p^*, P_{in,j})}{S_{VV,0}/\bar{n}_c(\omega_p^*, P_{in,0})}. \quad (\text{S8})$$

where the index $j = 0$ represents the low power regime where the $G = 1$.

³D. J. Newman. An l_1 extremal problem for polynomials. *Proceedings of the American Mathematical Society*, 16(6):1287–1290, 1965. ISSN 0002-9939. doi:10.1090/S0002-9939-1971-0280688-0.

⁴Daniel Bothner, Ines C. Rodrigues, and Gary A. Steele. Four-wave-cooling to the single phonon level in Kerr optomechanics. *Communications Physics*, 5(1):33, Feb 2022. ISSN 2399-3650. doi:10.1038/s42005-022-00808-3. URL <https://doi.org/10.1038/s42005-022-00808-3>.

³D. J. Newman. An l_1 extremal problem for polynomials. *Proceedings of the American Mathematical Society*, 16(6):1287–1290, 1965. ISSN 0002-9939. doi:10.1090/S0002-9939-1971-0280688-0.

⁴Daniel Bothner, Ines C. Rodrigues, and Gary A. Steele. Four-wave-cooling to the single phonon level in Kerr optomechanics. *Communications Physics*, 5(1):33, Feb 2022. ISSN 2399-3650. doi:10.1038/s42005-022-00808-3. URL <https://doi.org/10.1038/s42005-022-00808-3>.